PROGRESSIVE DAMAGE CHARACTERIZATION OF STITCHED, BI-AXIAL, MULTI-PLY CARBON FABRICS COMPOSITES

M. Vettori[1], T. Truong Chi[2], S. V. Lomov[2], I.Verpoest[2]

[1] Dipartimento di Ingegneria Industriale, Università degli studi di Parma.
Parco Area delle Scienze, 181/A – 43100 Parma, e-mail: vetto@me.unipr.it
[2] Material Engineering Department – Katholieke Universiteit Leuven

ABSTRACT

Plates of Biaxial Multiply carbon fabric has been produced with RTM process. Particularity of this new family of material is the presence of a stitching yarn that keep the position of the stacked layers of reinforcement, maintaining their position and orientation. The results of the mechanical characterization of the material is reported together with the characterization of its geometry. NDT investigation (acoustic emission, ultrasonic scanning and radiography) of the damage evolution and its characterization are described and results discussed.

1. INTRODUCTION

Fibre reinforced composite materials are widely used in military and aerospace industries, and in such applications in which high costs are justified by increased performances of the final product (i.e. racing cars, highend automotive products, etc.). Major advantages offered by this materials are an high stiffness-to-weight and resistance to weight ratios and high flexibility of use, that allows the customisation of material properties in relations to final product requirements. The traditional way to produce composite parts, where the fibre lay-up is fully controlled, is the *Autoclave* process, whose cost penalties are well discussed in [1].

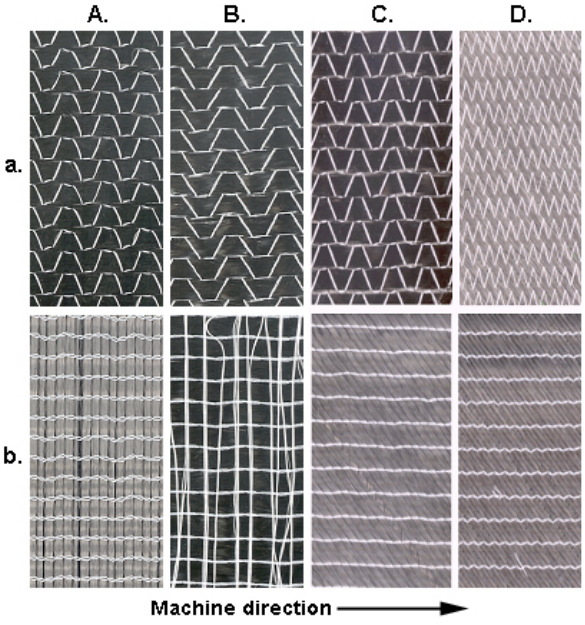

Fig. 1: Multi-axial Multi-ply Carbon Fabrics.

In recent years, the interest of composite manufacturer has been attracted by partially stacked UD fibre-reinforced composite materials. This new family of textiles (Fig. 1), well known as knitted fabrics, and referenced as multi-axial multi-ply fabrics (MMFs), overcomes many of the problems related to the use of unidirectional prepregs [1], [2]. These fabrics are made of unidirectional plies stacked sequentially in a number of possible orientations relative to the fabric warp direction. Individual plies are kept together by stitching yarns [3], [4]. The particular architecture of these materials, characterized by the nominal absence of fibre curvature, overcomes the crimp factor problem, providing full use of fibre mechanical properties.

The considerable reduction in price of carbon reinforcement, thanks to the use of heavy tows, has opened the possibility for multi-axial multi-ply carbon fabric (MMCF) to be used in more common applications [5]. To assess possible applications of this promising MMCFs, material properties as well as damage mechanics investigation are needed.

Experimental work to determ the internal geometry, the mechanical properties and investigation of damage development of MMCF reinforced epoxy composite is ongoing [4], [6], [8]. This paper, presents the results of progressive damage characterization of bi-axial (0-90°) multi-ply carbon fabric (BMCF), under static loads at different strains. Acoustic emission records, together with X-ray radiography and Ultrasonic scanning are used to evaluate and characterize damage. This work is closely related to [9].

2. MATERIALS AND COMPOSITE PRODUCTION.

The bi-axial multi-ply carbon reinforcement fabric was provided by Saertex Wagener GmbH & Co. Germany, and its characteristics are reported in Table 1. Two layer of unidirectional carbon fibers are stacked in 0/90° sequence, and stitched together with polyester (PES) yarn with tricot-warp pattern.

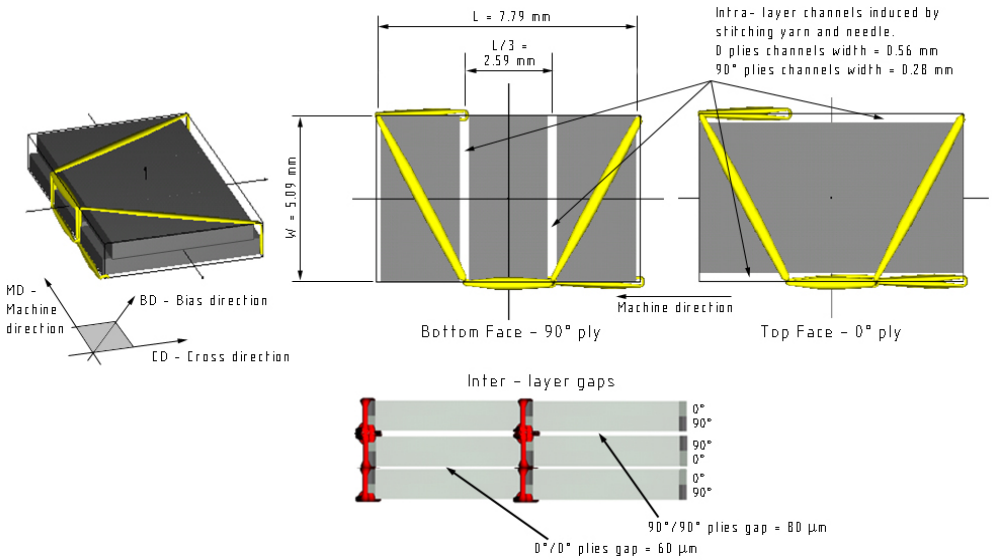

Fig. 2: Biaxial multi-ply carbon fabric nominal architecture and geometry. Unit cell and stitching induced defects are represented together with their averaged dimensions.

Table 1. The specifications of bia-axial multiply carbon fabrics.

Biaxial multi-ply carbon fabric (BMCF)	*Seartex Code*	*Plies orientation*	*Reinforcement material*	*Stitching material*
	V 92934-00310-01270	0/90°	24K, T600 Carbon fiber	PES stitching, 7.6 tex
Areal Density (g/m²)	*Biaxial Textile*	*Single UD layer*	*Stitching*	*Stitching Pattern*
	307 ± 5%	150 ± 5%	6 ± 5%	Tricot-Warp

Table 2. RTM Process' parameters. The injection pressure varies during the process: p_0 is the initial low injection pressure, maintaned for about 2 minutes to ensure a slow resin flow, in order not to damage excessively the material in correspondance of the injection point. After the injection a first cure process is done in the mold, than, after plate demolding, the final cure is done at high temperature in a oven.

Injection				***1st Cure***		***2nd Cure***	
T	40°C	**t**	20 ÷25 min	**in the mold**		**in oven**	
Initial injection pressure - p_0			2 bar	**T**	60 min	**T**	60 min
Injection pressure - p_1			3÷4 bar	**t**	70° C	**t**	160° C
Mold vacuum			- 0.4 ÷ 0.6 bar				

As discussed in [4], stitching creates disturbance on the uniform placement of the fibers. The action of the stitching needle, and the presence of the yarn introduces in the fabric some defects such as "cracks", "channels" and "gaps" when laying up the fabrics together. All of them can cause resin rich regions in the composites that can affect the mechanical performance, and the damage initiation and evolution mechanisms under loads. Characteristic dimensions of the elementary cell of the material, corresponding with the stitching characteristic dimensions are presented in Fig. 2, together with disturbances dimensions.

Shell epoxy resin Epikote 828 LV, mixed with 100/17 weight ratio, with hardener Epikure DX 6514 (supplied by EADS - European Aeronautic Defence and Space Company) were used as matrix system.

For composite production, the RTM equipment. RTM Process parameters are reported in table 2. Plates produced are obtained with 8 fabrics (16 plies) stacked symmetrically in a

$[0/90, 90/0, 0/90, 90/0]_S$ lay-up. The plates were cut using a diamond saw, into specimens with dimensions accordingly to the ISO 527-4 standard.

3. EXPERIMENTAL PROCEDURE.

In order to characterize damage evolution under quasi-static loads, different techniques has been applied for accurate damage identification.

Initially, acoustic emissions (AE) were recorded during preliminary tensile tests performed accordingly with the ISO 527-4, onto a 100kN Instron 4505 tensile testing machine. An extensometer with a 50 mm gage length was applied centrally to the specimen, together with two acoustic transducers placed at a relative distance of 110 mm, along the load direction (Fig. 3).

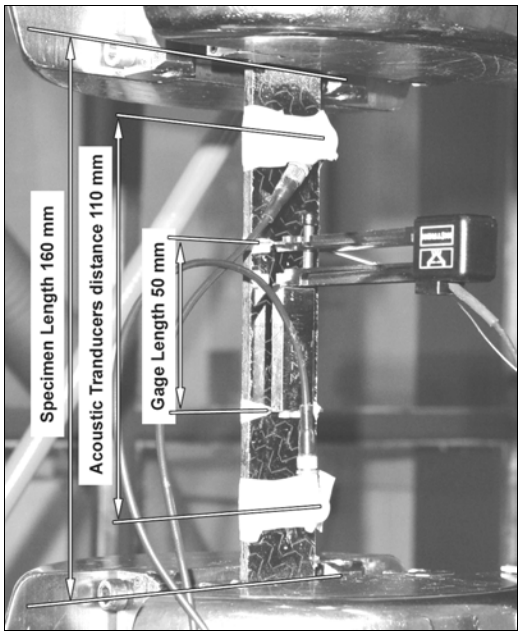

Fig. 3: Instrumented specimen.

Table 3: Set up parameters of acoustic emission, C-Scan and X-Ray equipments. ([1]) for both channels; ([2]) applied to conditioned signal.

Acoustic Emission (Digital Wave)	Preamplifier, dB	20
	High pass, kHz ([1])	20
	Low pass, kHz ([1])	4000
	Gain, dB ([1])	33÷39
	Trigger Gain, dB ([1])	33÷39
	Threshold for trigger, V ([2])	0.2
	Sampling rate, kHz	5
	Signal length (samples)	4096
	Pre-trigger buffer (samples)	512
C-Scan (Pulse-Echo mode)	Transducer, MHz	5
	Gate Position, μs	51
	Gate Width, μs	5
	Volts de-multiplier, V	0.2
	Amplification, dB	63
	Maximum XY resolution, mm	0.0375
X-Ray (Philips HOMX 161)	Voltage, kV	80-100
	Intensity, A	0.3
	Iris, %	80

The tests were carried out in different directions defined relatively to the fabric production process (Fig. 2): machine direction (MD) – corresponding to the 0° layer direction; cross direction (CD) – corresponding to the 90° layer direction and bias direction (BD) – corresponding to the ±45° direction. In Fig. 4 typical stress-strain curves are presented together with AE events counts, event energy and cumulative energy parameters. For now is sufficient to observe that for each curve it is possible to identify three different regions accordingly to AE event frequency (see 4.1 for detailed discussion). In order to characterize damage process and identify damage modes at different strain levels, into each one of this strain fields, for each test direction, a particular strain level has been chosen. Six tensile tests were then carried out until each strain level, along each test direction. X-ray radiographies and ultrasonic scans (USS) were then used onto the damaged specimens in order to reveal and identify damage.

In Table 3 are presented the set up parameters of AE, X-ray and USS apparatuses. For AE recordings a Digital Wave instrumentation was used, in bundle with Wave Explorer software, for real time events recording and further analysis. Two piezoelectric broadband acoustic transducers were used. X-Ray radiographies were then carried out with a Philips HOMX 161 system together with AEA Tomohawk software. In order to better localize damage and to obtain more contrast on radiographies, diiodomethane was used as contrast medium, applied to the specimen by a 24 hours bath. Radiographies were then acquired with a 12 bit CCD camera with a 1024 x 1024 pixel resolution, and a shutter speed of 25 frame/s. Ultrasonic

scans were taken using a pulse-echo, HFUS 2000 ultrasonic system, linked with a LeCroy 9400A dual 175MHz digital oscilloscope, and driven with a desktop PC.

4. PROGRESSIVE DAMAGE CHARACTERISATION

4.1 Acoustic Emission

As already introduced, Fig. 4 presents the information obtained from tensile tests coupled with AE records on 0°/90° laminates, along machine (Fig. 4.a), and bias (Fig. 4.b) directions; AE counts, stress, event energy and cumulative AE energy are plotted versus strain. Plots along cross direction, are essentially similar to the one along machine direction.

Three main regions may be identified observing the charts. At the very beginning of the test, for each test direction, few events of low energy contents occurs with very low frequency. Analogous results were obtained by Johnson at al [7] on epoxy/glass fibre cross-ply laminates. It indicates that micro damage occurs from already low strain levels.

Very closely after these events, at a typical transition strain (indicated as ε_a in Fig. 4) of 0.2% for machine and cross direction, and 2% for bias direction, the frequency of events increase suddenly and the energy content reach higher levels. This field of behaviour, characterized by a constant rate of events, covers a wide range of strains, until high deformations. In bias direction, as indicated by stress-strain charts, accordingly to previous observations [8], the stiffness of the specimen decrease rapidly in the initial region, and from the transition strain it progressively reaches a constant value. For the test in machine and cross direction (Fig. 4.a), stiffness of the material slightly increases despite of micro damage. It is because in this direction, the laminates are fibre-dominated materials and the contribution of matrix to overall stiffness is minor. As we will discuss later, the early damage, prior final failure, is mainly matrix cracks and local delamination hence it doesn't significantly reduce the material stiffness. The stiffness reduction due to matrix cracks is than compensated by stiffness increase due to the increase of carbon fibre stiffness under stretching. In bias direction, instead, the material is matrix dominated and matrix cracking or delamination strongly reduce the stiffness of the material.

At higher strain levels is possible to identify a transition strain field (indicated as ε_b in Fig. 4) that separate region two and region three of the charts. For machine and cross direction it is between 1.3 ÷ 1.4% and for bias direction 10 ÷ 12%. In the third region the damaging behaviour of the material depends on the test direction. Along MD and CD the frequency of the events tends usually to increase unstable, till the final collapse of the specimen. On the other hands, along BD direction, the frequency of events may stay constant till final failure, or progressively decrease until the final separation of the specimen into two parts.

Observing cumulative energy plots, along all test directions can be appreciated a repetitive behaviour while crossing the transition strains ε_a and ε_b. At the beginning of the test the energy content of first events is very low. Near ε_a events starts to release higher energy levels, and the cumulative energy plot show a positive concavity. Moving to higher strains, near the centre of the second region of the charts, the energy plot change progressively its behaviour stabilizing itself to a constant value. It shows that damaging mechanism get saturated towards ε_b. Again, getting closer to transition strain ε_b, the cumulative energy plot starts again to grow, generally quicker than at ε_a, with an unstable trend that leads to the final specimen collapse.

4.2 Ultrasonic and X-Rays observations.

As introduced, to inspect the initial damage and damage development, tensile tests were performed on the material at three different strain levels: $\varepsilon_1 = 0.2$ %, $\varepsilon_2 = 0.8$ % and $\varepsilon_3 = 1.3$ % in machine (MD) and cross direction (CD), and $\varepsilon_1 = 1$ %, $\varepsilon_2 = 6$ % and $\varepsilon_3 = 9.8$ % in bias direction (BD) (Fig. 4). In Fig. 5 and Fig. 6, the progressive damage analysis results from ultrasonic scanning (USS) and X-ray radiographies are presented respectively, for each test direction. In *machine direction*, accordingly with AE results, it is possible to identify some

micro matrix cracks since strain ε_1 [1]. These generally few cracks, are always oriented transversally and starts from one edge of the specimen as shown in the detail box of Fig. 6, MD-ε_1 picture.

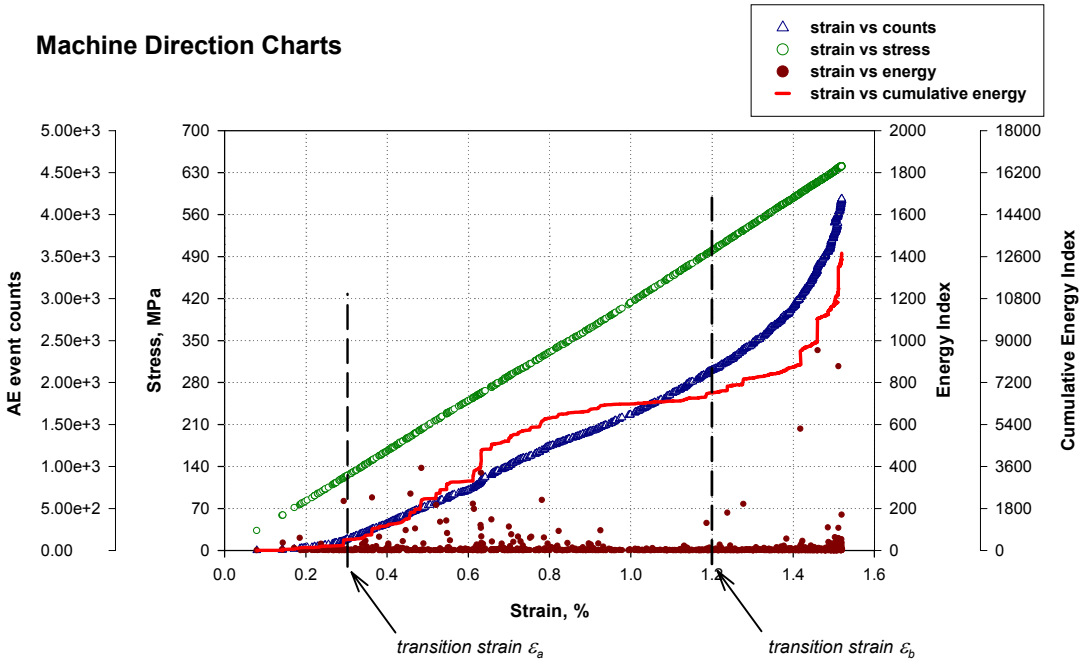

4.a

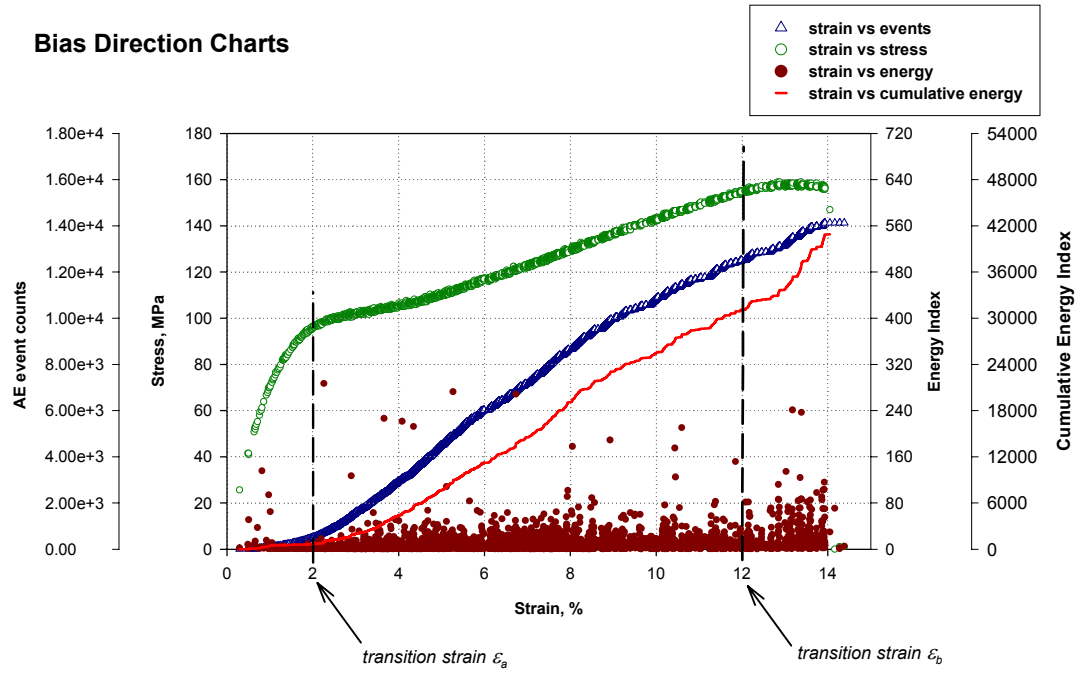

4.b

Fig. 4. Stress and strain curve together with acoustic emission counts, events' energy for machine and bias directions. Charts in cross direction are similar to machine direction charts.

They are probably small initiations of not yet fully developed matrix cracks as described by Johnson when he examined the damage development of 0°/90° laminates made from UD prepregs [7]. Increasing the strain level at ε_2, initial micro matrix cracks multiply themselves

[1] Micro cracks are difficult to be detected by ultrasonic technique, but they are quite well localized with X-ray radiographies in-spite of they small size.

and grow into transversal matrix flaws typically interesting the whole width of the specimen. Moreover, bigger cracks (whiter transversal flaws in Fig. 5, MD-ε_2 picture and darker ones in Fig. 6 MD-ε_2 picture) are surrounded by some delaminated regions identified by USS technique with areas of low intensity grey pixels around whiter transversal lines (Fig. 5, MD-ε_2 picture). Transversal cracks are dominant over longitudinal cracks, in-spite of some micro longitudinal defects that can be identified. At higher strain (ε_3), when the transverse matrix cracks are saturated, longitudinal cracks, due to fibre splitting mechanism, increase and grow, together with delaminations.

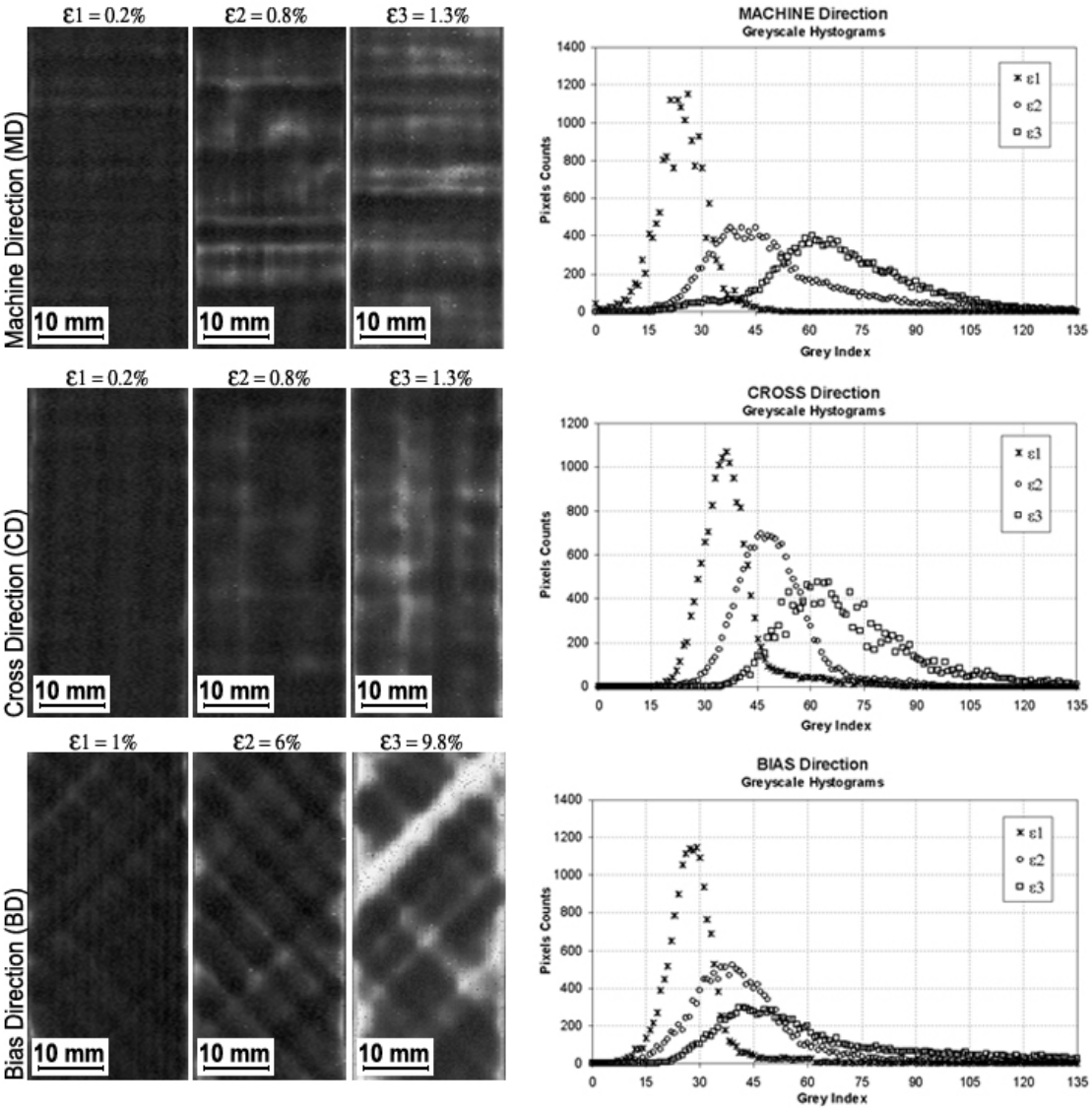

Fig. 5. Ultrasonic scanning results. In the left part are presented the greyscale images for test directions and different strain levels. Images are cropped within the gage length of the tests, i.e. with dimension (L×W) 50×25 mm. On the right are presented for each test direction three histograms of a single test at different strains.

In *cross direction*, similar damage process is involved. At strain ε_1 some longitudinal micro-matrix cracks are detected, here starting both form the edges and from the inside of the specimen (Fig. 6 CD-ε_1). They increase rapidly in number and dimensions at strain level ε_2, till strain level ε_3, where some longitudinal cracks may be detected. Moreover some delaminations can be identified by USS images growing both along transversal and longitudinal direction.

For the test in *bias direction*, at lower strain (ε_1) matrix cracks along fibres, beginning with cracks in +45° relative to loading direction, are observed (Fig. 5 and Fig. 6, BD-ε_1 pictures). At higher strain (ε_2), these matrix cracks develop increasing in number and forming longer cracks oriented both in +45°/-45° relative to loading direction. Most of them run from one edge of the specimen to the other. Small delaminations develop from the edges following existing matrix cracks. Some delaminations are generated also from inside the specimen, at crossing of +45°/-45° matrix cracks, as revealed by whiter spots in Fig. 5, BD-ε_2 picture. Increasing the applied strain towards the end of the test (ε_3), one or more of the delaminations grow interesting the whole width of the specimen, generating specimen failure.

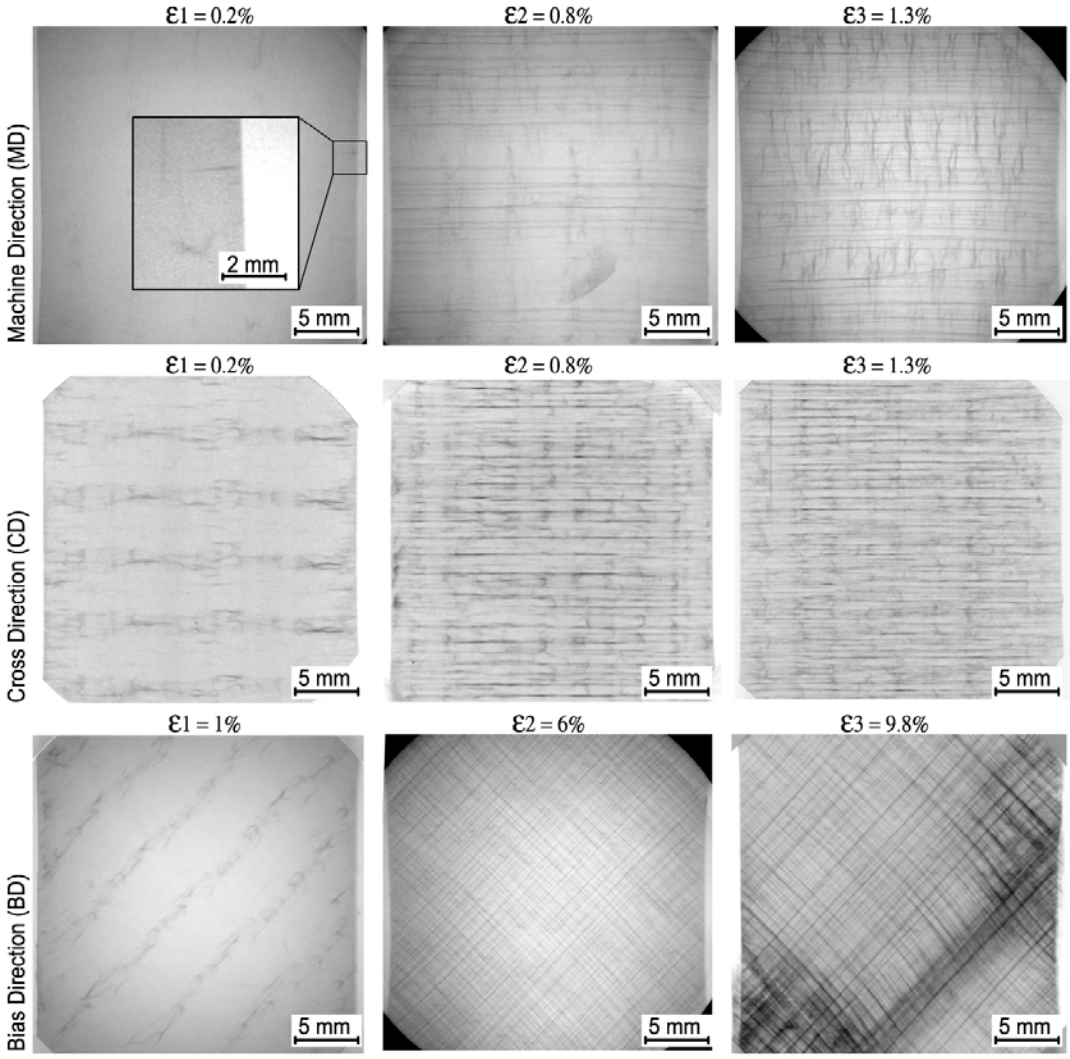

Fig. 6. X-Ray Radiographies. Images are taken in the centre of the specimen, inside its gage length, with dimension (L×W) 25×25 mm approximately.

To characterise the damage evolution integrally, it is useful to analyse greyscale histograms from USS images. Taking a window of the specimen coincident with the extensometer gauge length (W×L = 25×50 mm), greyscale histograms have been calculated for each test direction at each strain level. In Fig. 5, beside USS images, are presented the resulting histograms for each test direction (for the sake of clarity only one histogram for each strain level is presented). Damaged regions appear whiter on the USS images so that the number of "white" pixels, whose grey scale is above a threshold, can be used as an estimation of damage extension. Generally, as applied strain increases, the peak of histogram decreases, while its width increases, moving also toward higher grey indexes, meaning that the image is getting "whiter". Observing the histograms at ε_1 strain level, the grey intensity of pixels is generally in a range between 20 and 60 for each test direction, that is too low and narrow to create

sufficient contrast to localize and quantify damage, therefore it is very difficult to localize and quantify initial damage by USS. At strain level ε_2, the histogram move towards higher grey intensity values, getting wider and consequently with a lower peak. This is because of damage development in the specimen. According to Johnson [7], the initial micro matrix cracks starts to grow just before the knee on the events vs strain curve, at a typical transition strain level ε_a (Fig. 4), and continue until saturation is reached. This process develops increasing the length and the number of cracks in the specimen, increasing then the white intensity in USS images. As shown along MD and CD, cracks develop mainly parallel to fibres oriented in 90° relative to load direction, and present some small delaminations around major defects. In BD, cracks are oriented both in ±45° relative to load direction, with delaminated regions both inside and along edges. These different modes of damage in the specimens are related to their own grey scale registered on USS images, resulting in lower pick and wider the histogram.

Similar explanation applies for the histogram of the tests at ε_3, since there are also different modes of damage in the material. Along MD and CD longitudinal cracks and delaminations becomes leading mechanisms, while in BD, toward the end of the test matrix cracks along fibres and delamination can be seen (Fig. 5, BD-ε3 image). As strain increases, those cracks and delamination in specimens become larger leading to higher average grey scale of image, attributed to the shift of histogram toward higher grey value. Their high contrast makes it possible to observe damage easily from the USS images.

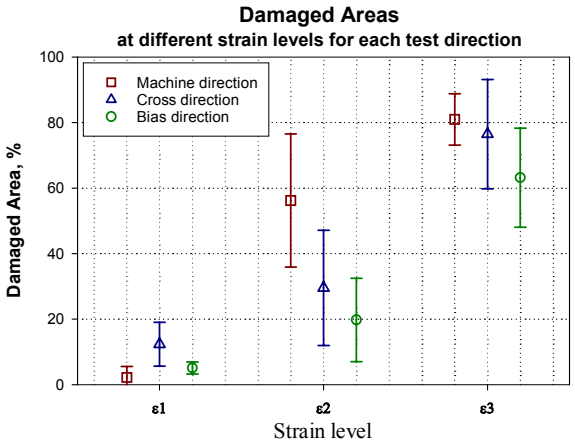

Fig. 7. Results from damage area calculations, presented for each test direction and strain level.

Moreover, the "damaged area" of the specimen can be measured quantitatively applying a threshold filter to USS cropped images. In order to have reliable indication on "damaged area", one undamaged specimen in machine direction has been chosen as reference. Its USS histogram fit well with a Gauss distribution of average value 34 and standard deviation 4.9. In order to calculate damaged area, a threshold value of 49 (mean + 3 standard deviation, i.e. the 99% of the histogram pixels), has been used for image filtering, results presented in Fig. 7.

For test along *machine* and *cross direction* at strain level ε_1, damaged area is close to 0, and damages are seen mainly near the edges of the specimen (Fig. 5). It is believed that the detected damage at ε_1 is due to edge effects, which is not the case in a structure. Therefore damaged area along MD and CD, can be assumed as zero. Along *bias direction* damaged area at ε_1 is bigger than in MD and CD, and some damage can be detected also from inside the specimen. Damage at ε_1 along bias direction, cannot be neglected: although some damage is imputable to edge effects, some developing micro matrix cracks may be appreciated, too.

It is quite logical to observe "damaged area" increasing when applied strain increases along each direction. However, in MD and CD, damage increases gradually with the applied strain, while along BD it increases more slowly at low strain levels, and faster going form ε_2 to ε_3. This behaviour it is due to the significant contribution of the delamination mechanism, that in bias direction, after a certain strain level, it is the main damage mode. Delamination was also observed by eyes on the surface layers of the specimens.

4.3 Damage periodicity investigation.

Observing the images presented in Fig. 5 and Fig. 6, some periodicity in damage may be appreciated. In order to investigate the reasons of these periodicity a measurement of its typical dimensions has been carried out.

Periodicity can be well identified in USS images taken at strain ε_2. Different measuring lines has been drawn on these images aligned with load direction for MD and CD, and aligned at ±45° relative to load direction for BD (Fig. 8.a). Along the measuring lines the grey intensity value of the USS image pixels has been isolated and plotted (Fig. 8.b). The waveform that comes out from each measurement has been treated as a signal, and transformed with Fourier analysis, in order to evaluate its main frequencies (or periods). The final results (Fig. 8.c) is a group of characteristic distances between damaged areas, along the paths described by the different measurement lines. In order not to consider measurement noise, before processing the images, they have been submitted to average filtering with 3 pixels radius. Moreover, from the different periodicities evaluated, have been considered only those with amplitude within a relevance range of the 60% of the maximum amplitude, as shown in (Fig. 8.c). This analysis aim at appreciating damage periodicity inside each fabric, overcoming the effects of the stacking process, that create a phase error between different layers which are superposed shifted one in respect to the other. The results from Fourier analysis are summarized in Table 4, where the characteristic distances between damages for each test direction are reported.

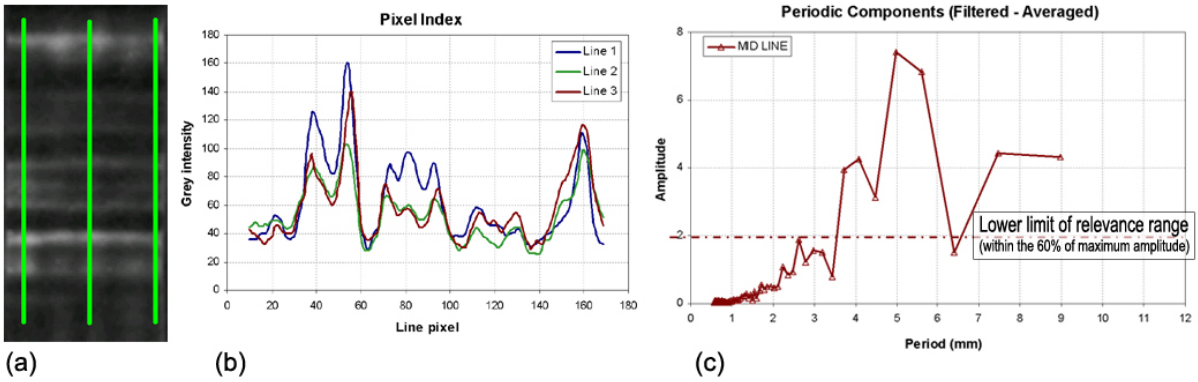

Fig. 8. Example of periodicity analysis in machine direction.

Table 4. Results of damage periodicity investigation, reported as averaged distances between damages along each test direction.

	1st period L1	2nd period L2	3rd period L3	4th period L4
MD	*2.63 mm*	*3.44 mm*	*4.97 mm*	*7.47 mm*
CD	*5.6 mm*	*n.p.*	*n.p.*	*n.p.*
BD (+45°)	*2.3 ÷ 2.77 mm*	*3.46 ÷ 4.61 mm*	*5.54 mm*	*6.93 mm*
BD (-45°)	*5.54 mm*	*n.p.*	*n.p.*	*n.p.*

Along the machine direction, damage periodicity length varies in a broad range, differently from cross direction where one characteristic length is dominant. Comparing these lengths with fabric's unit cell dimensions (Fig. 2) there correlation is good. L1 in MD is very close 2.59 mm that is the typical distance between subsequent needle holes. L4 in MD is also corresponding with the unit cell length in machine direction. L1 in CD is close to the width of the unit cell (5.09 mm – measured in cross direction relatively to the fabric).

These results show that the stitching pattern in the fabric is well correlated with the damage evolution pattern. As discussed in a previous paper [4], stitching creates resin rich pockets which may initiate cracks.

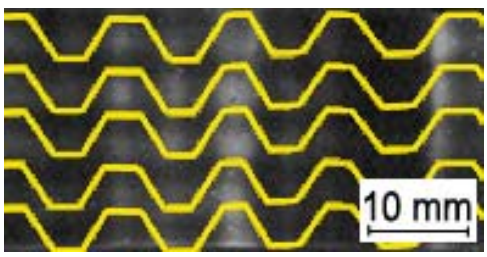

Fig. 9. Stitching pattern superposed with the damage pattern for a MD specimen.

Hence damages follows stitching pattern, in its growth process. This result is confirmed by superposition of stitching pattern onto the damage pattern obtained by USS technique, as shown in Fig. 9.
The relation between the stitching and damage is still subject of ongoing work to characterise damage in BMCF and MMCF laminates.

5. CONCLUSIONS

Damage initiation and development has been observed and studied along three different test directions, for Bi-axial Multi-ply Carbon Fabrics, by the mean of different non-destructive techniques. Starting from first results of Acoustic Emission records during standard tensile tests, damage evolution has been monitored versus applied strain. Three different damaging fields have been detected on the events vs. strain charts. Inside each one of these fields, tensile tests has been stopped at a significative strain level. Partially damaged specimens were then subjected to both Ultrasonic scanning and X-ray radiography. The damaged area at different strains has been evaluated by threshold filtering and periodicity on damage distribution into specimen has been revealed.
Present results about damage modes and mechanism agree with previous studies [7], [8]. By the mean of geometrical characterization of damage periodicity along load direction a close relation between stitching pattern and damage pattern has been demonstrated. Ongoing work is intended to asses this relationship, by the mean of geometrical analysis of the damage periodicity on radiographies and, along 90° relative to load direction, on ultrasonic scans. Future finite element damage analysis is also intended to numerically reveal stress concentration effects due to stitching disturbances.

ACKNOWLEDGEMENTS

This work was done in the framework of the projects "Technologies for Carbon Fibre Reinforced Modular Automotive Body Structures" (TECABS, Brite-Euram) and "Marie Curie Training site", funded by the European Commission, "Development of unified models for the mechanical behaviour of textile composites" (GOA/98/05), funded by the Flemish Government through the Research Council of KULeuven, "Vlir-CTU Institutional Universities Co-operation" funded by Flemish Government.

References

1. **Bibo, G. A., Hogg, P. J.** and **Kemp, M.**, "Mechanical characterisation of glass and carbon fibre reinforced composites made with non-crimp fabrics", *Compos Sci Technol*, **57** (1997) 1221-1241.
2. **De Luca, P.** and **Dufort, L.**, "Numerical tools for advanced composite materials: A mean to reduce costs and improve performance", *24th International SAMPE Europe conference*, (2003) 537-544.
3. Reinforcement Specifications for multi-axial multi-ply fabrics. CEN TC 249; 2000-07, prEN 13473-1.
4. **Lomov, S. V., Belov, E .B., Bischoff, T., Ghosh S. B., Truong C. T.**, and **Verpoest, I.**, "Carbon Composites Based on Multi-Axial Multi-Ply Stitched Preforms. Part 1: Geometry of the Preform", *Compos Part A-Appl S*, **33**, (2002), 1171-1183.
5. **Palmer., R. J.**, "Manufacture of Dry Fibre Preforms and Multiaxial Stitch Bonded Fabrics", P*roceedings of the 22nd International SAMPE Europe Conference*, Ed. G.R. Griffith and R.F.J. McCarthy, (2001) SAMPE Paris, 281-292.
6. **Truong, C.T., Lomov, S.V.** and **Verpoest I.**, "The mechanical properties of multi-axial multi-ply carbon fabric reinforced Epoxy composites" *Proceeding of the ECCM10*, Brugge-Belgium (2002).
7. **Johnson, M., Gudmundson, P.,** "Broad-band transient recording and characterization of acoustic emission events in composite laminates", *Compos Sci Technol*, **60** (2000) 2803-2818.
8. **Truong, C.T., Vettori, M., Lomov, S.V.** and **Verpoest I.**, "Multi-axial Multi-ply carbon fabric reinforced epoxy composites: mechanical properties and investigation of initial damage" *Proceedings of the ICCM 14*, Brugge-Belgium (2004).
9. **Truong, C.T., Vettori, M., Lomov, S.V.** and **Verpoest I.**, "New results on mechanical properties and initial damage of multi-axial multi-ply carbon fabric reinforced epoxy composites", *Accepted for ECCM-11 Poster presentation* (2004).